# A New Model for Contact Angle Hysteresis

**Antonio DeSimone, Natalie Grunewald,
Felix Otto**

**no. 280**

Diese Arbeit ist mit Unterstützung des von der Deutschen Forschungsgemeinschaft getragenen Sonderforschungsbereiches 611 an der Universität Bonn entstanden und als Manuskript vervielfältigt worden.

Bonn, Juli 2006

# A New Model for Contact Angle Hysteresis

Antonio DeSimone * Natalie Grunewald† Felix Otto ‡

**Abstract**

We present a model which explains several experimental observations relating contact angle hysteresis with surface roughness. The model is based on the balance between released energy and dissipation, and it describes the stick–slip behavior of drops on a rough surface using ideas similar to those employed in dry friction, elasto–plasticity and fracture mechanics. The main results of our analysis are formulas giving the interval of stable contact angles as a function of the surface roughness. These formulas show that the difference between advancing and receding angles is much larger for a drop in complete contact with the substrate (Wenzel drop) than for one whose cavities are filled with air (Cassie-Baxter drop). This fact is used as the key tool to interpret the experimental evidence.

**Keywords.**

PACS.68.08.Bc - Wetting.
PACS.68.03.Cd - Surface tension and related phenomena.
PACS.47.55.D- - Drops and bubbles.

**AMS Subject Classification Numbers.**

49S05 Variational principles of physics
76B45 Capillarity (surface tension)
74C05 Small-strain, rate-independent theories (including rigid-plastic and elasto-plastic materials)

*SISSA-International School for Advanced Studies, Trieste, Italy, desimone@sissa.it.
†Inst. für Angewandte Mathematik, Universität Bonn, Germany, grunewald@iam.uni-bonn.de.
‡Inst. für Angewandte Mathematik, Universität Bonn, Germany, otto@iam.uni-bonn.de.

# Contents



# 1 Introduction

We consider liquid drops resting on a rough solid surface. The angle at which the liquid/vapor interface meets the solid is the contact angle. While Young's law gives *one* value of this angle, the one associated with a drop minimizing the total interfacial energy, contact angle hysteresis shows that there exists a whole interval of stable contact angles. Both the end points and the width of this interval depend in a non–monotone way on the roughness of the solid, see the reviews [dG], [Q], and [dBQ]. Figure 1, taken from [DJ], shows some well known measurements of advancing and receding angles which bound the interval of stable contact angles (the *hysteresis interval*).

More recent experiments show that, even at constant roughness, there may be more than one value for the receding angle, depending on the details of the drop deposition process, see [LQ]. In fact, in Figure 2, a large pressure is exerted on a Cassie–Baxter (CB) drop (i.e., a drop which has vapor-filled cavities underneath) which turns it into a Wenzel (W) drop (i.e., a drop with complete contact with the underlying surface) inducing a dramatic change in the measured receding angle.

Furthermore, plants use roughness to make the surfaces of their leaves ultrahydrophobic (see [BN]) although their constitutive material might in principle even be hydrophilic. A mechanism by which roughness may lead to CB–drops with large contact angles on hydrophilic surfaces, in spite of their high cost in terms of surface energy, is discussed in [H].

We introduce a new model to capture these phenomena. It predicts a much narrower hysteresis interval for CB–drops than for W–drops. This can explain both the downward

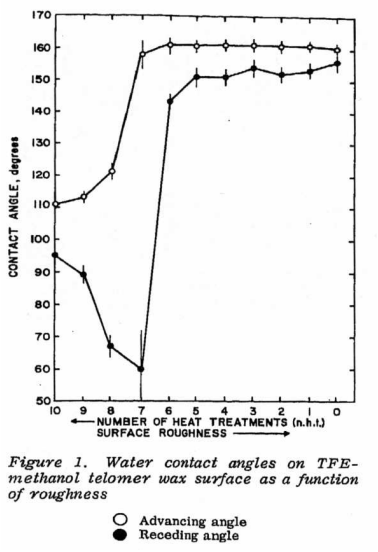


Figure 1: Experimental dependence of advancing and receding contact angles on the surface roughness. Reprinted with permission from [DJ]. Copyright (1964) American Chemical Society.

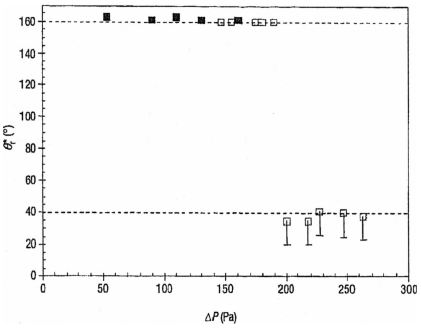


Figure 2: Experimental dependence of receding contact angles on the pressure pushing the drop onto the surface. Drops are of CB–type at low pressure and of W–type at high pressure. Reprinted from [LQ] with permission.

jump at large pressures of the experimental points in Figure 2, and the non–monotone behavior of Figure 1. The main result of this paper is the quantitative dependence of the hysteresis interval on the surface roughness and the type of drop. It is given both in terms of formulas (see Equations (7)–(9)) and in terms of stability diagrams (see Figures 6–8). Our model also leaves the possibility of metastable drops. That is, drops can be stable without minimizing surface energy. In fact, CB–drops can even be stable on hydrophilic surfaces and exhibit on them the large contact angles typical of super–hydrophobicity.

Our new model shares with similar ones used in dry friction [MT], fracture and damage mechanics [FM], [FG], and elasto–plasticity [DM] two main features. First, there is a critical "loading" that needs to be overcome before the system starts to dissipate energy. In our case, adding liquid to an existing stable drop (or tilting the surface on which a heavy drop sits) at first only changes the contact angle and the drop does not move. Surface energy is only dissipated after the drop starts moving. Second, the model is rate independent, i.e., the response of the system does not depend on the loading rate. Loading the system at a doubled rate will lead to the same response, at twice the speed.

The main idea behind our model is that the stability of a drop is not related to global or local minimality of its interfacial energy, but rather to the fact that the energy–landscape seen by a stable drop should not be too steep. More precisely: if the energy that would be gained by moving (i.e., the slope of the energy landscape) is smaller than the energy that

would be dissipated through the motion, then the drop will not move. Once the drop starts moving, the dynamics is controlled by the balance between available energy and energy dissipated through motion. Of course, we are here focusing on the quasi-static limit (no inertia) and on small drops (no gravity, and viscous dissipation inside the drop negligible with respect to dissipation at the moving contact line). On the other hand, we assume that the size of the asperities is much smaller than the size of the drops. In order to implement these ideas, we use the derivative–free framework proposed in [MM] (see also the review [M]).

Our model implies four different diagrams of stable contact angles, depending on the type of drop (W– or CB–type) and on the state of the surface in the vicinity of the contact line (dry or with puddles). It turns out that CB–drops are never stable when surrounded by water-filled cavities, while the three nontrivial diagrams are shown in Figures 6–8.
The model can also predict the time evolution under slowly changing external loads (e.g. the adding or removing of liquid). It identifies the microstructure (i.e., the microscopic pattern of contacts) with which the drop will advance or recede, which corresponds to the most unstable direction in the given energy landscape.

Our approach gives a qualitative explanation of the experiments mentioned above. Figure 1 can be understood as a superposition of the two stability diagrams for a dry surface. The highly non–monotone behavior of the width of the hysteresis interval comes from a transition from W–drops (Figure 6) to CB–drops (Figure 7). Indeed, using a notion of stability introduced in Section 3.2, one can show that, for the case of a dry surface, the stable configurations at low roughness are of W–type. At higher roughness, the stable configurations are instead CB , see Figure 9, and they display a much narrower hysteresis interval.
Figure 2 reflects the fact that the stability interval depends on the type of drop. Assuming that the corresponding surface is dry and has sufficiently large roughness ($r > r^*$ in the notation of Section 3), we see from Figures 6 and 7 that forcing a transition from a CB to W drop (by applying a large enough pressure) may reduce the lower end of the stability interval (i.e., the receding contact angle) from well above to well below $90^\circ$.
Our model can also reproduce the arguments in [H] in so far that CB–drops can be stable on a hydrophilic surface, although they do not minimize surface energy.

The rest of the paper is organized as follows. In Section 2, we describe the model in detail. In Sections 3 and 4, our results and their physical implications are discussed without proofs. These are deferred to Section 5.

# 2 A new model for contact angle hysteresis

## 2.1 Setup and notation

In the following we assume a 2–d setup, i.e., both surface and drops are infinitely extended along one direction (perpendicular to the plane of Figure 3). Although this assumption is not necessarily valid in experiments, see [dG], it is very useful in a first attempt to build some intuition.
The solid surface is described by a periodic step function $S : [-R, R] \to (-\infty, 0]$ for some sufficiently large $R \in \mathbb{R}_+$. $S(x)$ is the height of the solid at position $x \in [-R, R]$. The two relevant parameters for $S$ are its roughness $r$ (i.e. the length of the surface divided by the length of its horizontal projection) and its proportion of tops $\varphi < 1$, see Figure 3. It is normalized such that at the tops $S(x) = 0$, and its period is of length $\varepsilon \ll 1$.

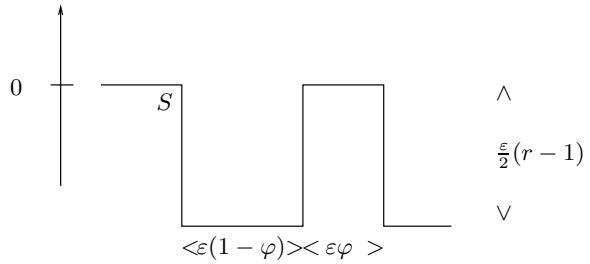


Figure 3: Microscopic roughness of the solid

This gives a generic surface, for which the area of contact with a drop can be easily determined: It is either the whole surface, or the tops without the cavities. This is a simplification with respect to smooth surfaces for which the wetted area needs to be computed by finding configurations meeting the wall cavities at the right microscopic contact angles. In this case, the proportion of wetted area $\varphi$ does depend on the exact shape of the surface. This, however, does not introduce new features to the model: it will lead to the same results, but with a variable $\varphi$.

Furthermore, we introduce a region near the solid: $RS := \{(x, y) \,|\, x \in [-R, R]\,,\, y \in (S(x), 0]\}$, see Figure 4, and the box: $B := [-R, R] \times (0, 1]$. Note that the height of $B$ can be chosen arbitrarily as long as it is much bigger than the periodicity of the microstructure of the solid (i. e. $\varepsilon \ll 1$). At time $t$ a drop is given by some subset $L(t) \subset \{B \cup RS\}$, where the liquid is located. A time dependent drop configuration is described by the function $L$ from $[0, \infty)$ into the subsets of $\{B \cup RS\}$.
We restrict our attention to drops which are of the following form (see Figure 4): The liquid is situated at the left side of $\{B \cup RS\}$. Inside $B$ the boundary of $L(t)$ forms a liquid/vapor interface which consists of a straight line. This line meets the solid at position $X(L(t))$ and the upper boundary of $B$ at position $Z(L(t))$. We call $X(L(t))$ the triple point and $Z(L(t))$ the upper interface point. The angle formed between the boundary of $B$ and the liquid/vapour interface at position $Z(L(t))$ is the contact angle $\theta(L(t))$. In the

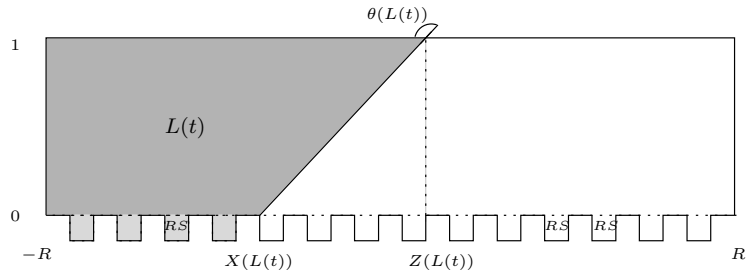


Figure 4: Drop configuration

region near the solid $L(t)$ can have two possible configurations: either W–type (the cavities $\{RS|_{x<X(L(t))}\}$ are all nonempty) or CB–type (the cavities $\{RS|_{x<X(L(t))}\}$ are all empty). These are according to Section 2.3 the only relevant drop configurations.
The boundary of $L(t)$ at the solid forms the solid/liquid interface $\Sigma_{S/L}$. The rest of $S$ is the solid/vapour interface $\Sigma_{S/V}$. And the rest of the boundary of $L(t)$ is the liquid/vapour interface $\Sigma_{L/V}$.

## 2.2 Energy and dissipation distance

The relevant free energy is the surface energy which consists of the energies of the three different interfaces. We consider this energy in nondimensional form, so that $\Sigma_{L/V}$ has energy per unit area one. The liquid/solid interface has energy per unit area: $-\cos\theta^Y$. Here $\theta^Y$ is the Young contact angle, which minimizes the surface energy on a flat solid. The solid/vapour interface has zero energy. Thus, the energy is given by

$$E\big(L\big) \;:=\; \big(|\Sigma_{S/L}|(-\cos\theta^Y) \;+\; |\Sigma_{L/V}|\big)\;, \tag{1}$$

where $|\Sigma|$ denotes the area of $\Sigma$. In the geometry of Figure 4, Equation (1) reads

$$E\big(L\big) \;=\; \big(|\Sigma_{S/L}\cap RS|(-\cos\theta^Y) \;+\; |\Sigma_{L/V}\cap RS|\big) \;+\; \sqrt{1+\big(X(L)-Z(L)\big)^2}.$$

To introduce an external loading we force the upper interface point to move in time. The time dependent energy is then

$$E\big(t,L\big) \;:=\; \big(|\Sigma_{S/L}\cap RS|(-\cos\theta^Y) \;+\; |\Sigma_{L/V}\cap RS|\big) \;+\; \sqrt{1+\big(X(L)\pm t\big)^2}.$$

We describe dissipation through the change in wetted solid area. This seems reasonable as it is well known that dissipation occurs mostly along the moving triple contact line. Thus, we define the energy dissipation in the time interval $[t_0,t_1]$ as

$$Diss\big(L,[t_0,t_1]\big) \;:=\; \lambda\int_{t_0}^{t_1}\int_{-R}^{R}\Big|\frac{d}{dt}\chi\big(\Sigma_{S/L}(t)\big)\Big|\,dSdt \tag{2}$$

where $\lambda \geq 0$ is a phenomenological material parameter, $\chi(\Sigma_{S/L}(t))$ is the characteristic function of the time dependent solid/liquid interface and $dS$ denotes integration along the solid surface. The distance between two configurations is the minimal energy dissipated along a path joining them:

$$dist(L_0, L_1) := \inf_L \left\{ Diss\big(L, [0,1]\big) \,\middle|\, L(0) = L_0,\ L(1) = L_1 \right\}.$$

The infimum is achieved for monotone $L$. Thus, the distance between two drops is the length of the solid wetted by only one of them:

$$\begin{aligned} dist(L_0, L_1) &= \lambda \int_{-R}^{R} \left| \chi(\Sigma_{S/L}(L_1)) - \chi(\Sigma_{S/L}(L_0)) \right| dS \\ &= \lambda \left| \left\{ \Sigma_{S/L}(L_1) \cup \Sigma_{S/L}(L_0) \right\} \setminus \left\{ \Sigma_{S/L}(L_1) \cap \Sigma_{S/L}(L_0) \right\} \right|, \end{aligned} \tag{3}$$

where $\Sigma_{S/L}(L_i)$ denotes the solid/liquid interface of the configuration $L_i$. This distance is macroscopically proportional to the usual distance between the two triple points.

## 2.3 Model for the stability of contact angles

We look at a single drop $L_0$. To model the observed hysteresis we relax the condition that a stable drop is a local minimizer of the energy (leading to Young's law). Instead we only require $L_0$ to be stable in the following sense:

$$E(L_0) - E(\tilde{L}) \leq dist(L_0, \tilde{L}) \tag{4}$$

for all $\tilde{L}$ which agree with $L_0$ on the upper boundary of $B$, i.e. on $\partial B \setminus \{[-R, R] \times 0\}$, but can have different contact angles. This is a global condition on the amount by which the energy can be reduced by changing $L_0$. Locally it says that the slope of the energy landscape at $L_0$ must not be too steep for $L_0$ to be stable. In fact, $E(L_0) - E(\tilde{L})$ has to fit under the cone $dist(L_0, \tilde{L})$, see Figure 5. It is crucial for $dist$ to be homogeneous of degree one. This leaves some freedom for the slope at a stable point to be non zero.

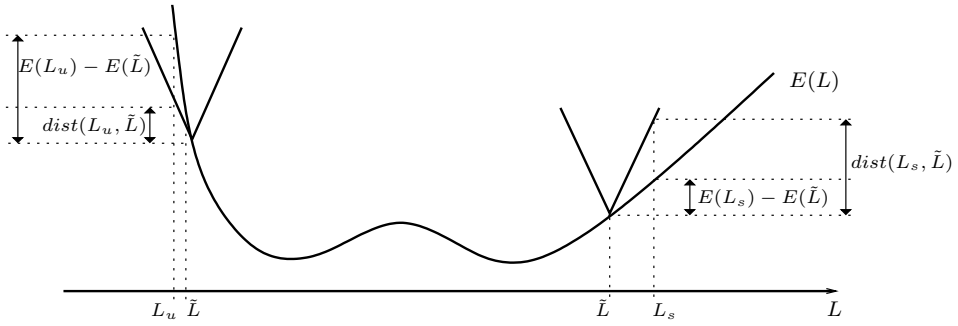


Figure 5: Energy landscape and dissipation distance

Furthermore, it is now clear that it suffices to consider drops whose liquid/vapour interfaces are straight lines. Drops with curved interfaces are unstable in the sense of (4) since straightening the interface reduces the energy without creating new distance.

## 2.4 Model for quasistatic evolution

External loading induces a change in the droplet configuration, as the energy becomes time dependent. This may lead to instabilities, and the system will jump to a new stable configuration. Following [MM, Definition 2.1], we consider time evolutions $L$ satisfying two conditions. First, at every time $t \in [0,\infty)$ the drop $L(t)$ has to be stable, i.e.:

$$E\big(t, L(t)\big) \;-\; E\big(t, \tilde{L}\big) \;\leq\; dist\big(L(t), \tilde{L}\big) \tag{5}$$

for all $\tilde{L}$ which agree with $L(t)$ on the upper boundary of $B$.
Second, the dissipation of energy has to balance the energy difference together with the change in external loading:

$$E\big(t_1, L(t_1)\big) \;-\; E\big(t_0, L(t_0)\big) \;+\; Diss\big(L, [t_0, t_1]\big) \;=\; \int_{t_0}^{t_1} \partial_t E\big(s, L(s)\big)\, ds \tag{6}$$

for all $t_0, t_1 \in [0,\infty)$, and for $Diss$ as defined in (2).

# 3 Results

## 3.1 Stable contact angles

The model introduced in Section 2.3 gives four different diagrams for stable contact angles depending on the type of drop (Wenzel or Cassie–Baxter) and on the state of the surface on which it is resting (dry surface or surface with puddles). These diagrams (Figures 6–8) are plotted for the most interesting case, namely, under the assumption that $-\cos\theta^Y - \lambda < 0 < -\cos\theta^Y + \lambda$. It will turn out that this assumes for the flat surface the advancing resp. receding contact angle to be above resp. below 90°. We use the following notation

$$\begin{aligned} r^* \;&:=\; \frac{1-\varphi}{-\cos\theta^Y + \lambda} + \varphi, \\ r^{**} \;&:=\; \frac{1-\varphi}{\cos\theta^Y + \lambda} + \varphi, \end{aligned}$$

which gives $r^* < r^{**}$ for the hydrophobic case $-\cos\theta^Y > 0$ (the case shown below) and vice versa.
Figure 6 shows the negative cosines of the stable contact angles depending on the roughness $r$ for the case of W–drops on a dry surface. The region of stability is obtained from four bounds, which come from (4) by comparing with different types of test drops $\tilde{L}$. For the two upper boundaries, $W/D$ and $CB/D$, the instability arises because the contact angle is too big. Therefore it is energetically advantageous to advance along the solid, i.e. the relevant comparison configurations $\tilde{L}$ in (4) are drops which have already advanced. The newly wetted area can have two different types of microstructure: either W– or CB–type. Advancing with W–type microstructure gives instability if $-\cos\theta \geq W/D := r(-\cos\theta^Y + \lambda)$. Whereas

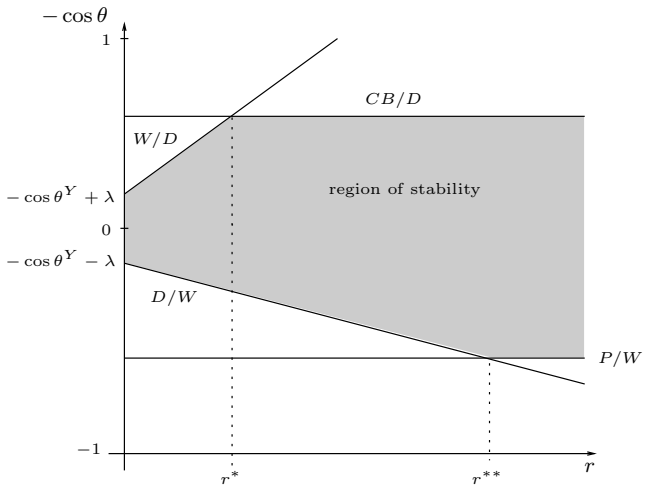


Figure 6: Stable contact angles for Wenzel drops on a dry surface

advancing with CB–type implies instability if $-\cos\theta \geq CB/D := \varphi(-\cos\theta^Y+\lambda)+1-\varphi$. The two lower bounds, $D/W$ and $P/W$, arise because the contact angle is too small. It is energetically better to recede from some area previously wetted. There are two possibilities to dewet area. Either the surface left behind is dry ($D/W$) or there are puddles on it ($P/W$). This gives instability if $-\cos\theta \leq D/W := r(-\cos\theta^Y-\lambda)$ and $-\cos\theta \leq P/W := \varphi(-\cos\theta^Y-\lambda)-1+\varphi$.

Summarizing, the hysteresis interval for a Wenzel drop on a dry surface is given by

$$-\cos\theta \in \begin{cases} \big(r(-\cos\theta^Y-\lambda)\,, r(-\cos\theta^Y+\lambda)\big) & \text{if } r \leq r^*\,, \\ \big(r(-\cos\theta^Y-\lambda)\,, -\cos\theta^{CB}+\lambda\varphi\big) & \text{if } r^* \leq r \leq r^{**}\,, \\ \big(-1+\varphi+\varphi(-\cos\theta^Y-\lambda)\,, -\cos\theta^{CB}+\lambda\varphi\big) & \text{if } r^{**} \leq r\,, \end{cases} \tag{7}$$

where $-\cos\theta^{CB} := 1-\varphi-\varphi\cos\theta^Y$. Notice that (7) provides $\lambda$ with a physical interpretation, namely, that of half the hysteresis interval for an ideally flat ($r=1$) surface.

Our model implies a different diagram for CB–drops on a dry surface, see Figure 7. The advancing (upper) bounds are the same as for W–drops, as the microstructure under the drop does not play a role for advancing variations. The bound for advancing with W–type microstructure is not relevant as we get a new bound $I$ which comes from interior variations. That is, we compare the drop $L_0$ of CB–type with a drop $\tilde{L}$ which wets the cavities underneath $L_0$, and obtain that CB–drops are never stable for $r < r^*$. For receding variations it is only relevant to recede with a dry surface. We get instability if $-\cos\theta \leq D/CB := \varphi(-\cos\theta^Y-\lambda)+1-\varphi$.

Summarizing, the hysteresis interval for a Cassie–Baxter drop on a dry surface is given by

$$-\cos\theta \in \big(-\cos\theta^{CB}-\lambda\varphi\,, -\cos\theta^{CB}+\lambda\varphi\big) \quad \text{for } r \geq r^*, \tag{8}$$

which gives a narrower hysteresis interval than for the flat surface, as $2\lambda\varphi < 2\lambda$. In the limit $\varphi \to 1$ we have $r^* \to 1$ and the hysteresis interval tends to $(-\cos\theta^Y-\lambda, -\cos\theta^Y+\lambda)$

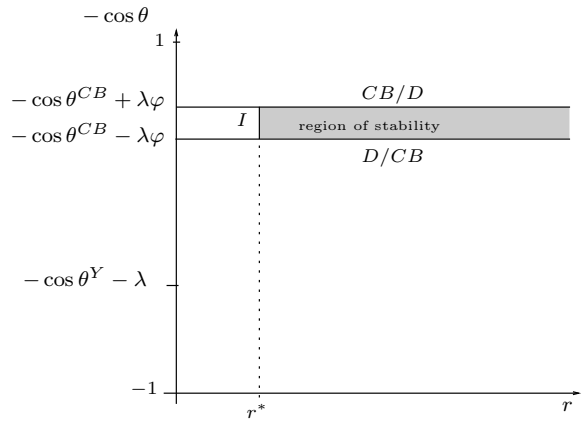


Figure 7: Stable contact angles for Cassie–Baxter drops on a dry surface

which is the interval for the flat surface ($r = 1$). On the other hand in the limit $\varphi \to 0$ of small areal density of solid tops, $-\cos\theta^{CB} \to 1$ and the width of the hysteresis interval tends to zero. The material behaves ultrahydrophobic. Notice that Diagram 7 and Equation (8) are valid independent of the sign of $\cos\theta^Y$ (hydrophobic or hydrophilic material).

We now turn to drops on a surface with puddles. Figure 8 shows the stable contact angles for W–drops on such a surface.

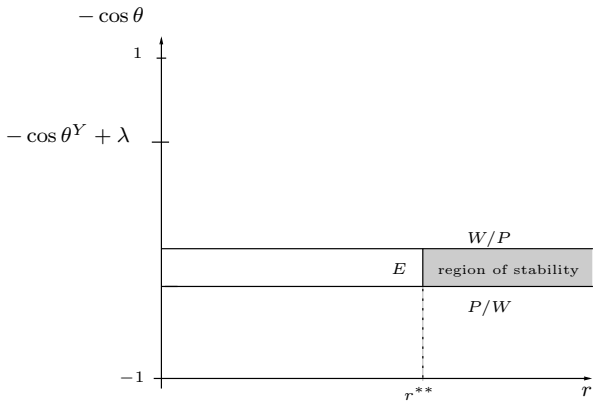


Figure 8: Stable contact angles for Wenzel drops on a surface with puddles

The bound $W/P := \varphi(-\cos\theta^Y+\lambda)-1+\varphi$ comes from advancing with W–type microstructure. For receding from wetted area we get the same bounds as for the dry surface because the surface structure is unimportant for receding from wetted area. The bound $D/W$ does not play any role since there exist destabilizing exterior variations $E$ (i.e., removing one of the puddles on the surface) which imply that puddles on a surface are instable for $r < r^{**}$. Summarizing, the hysteresis interval for a Wenzel drop on a surface with puddles is given by

$$-\cos\theta \in \big(-1+\varphi(-\cos\theta^Y-\lambda+1)\,,-1+\varphi(-\cos\theta^Y+\lambda+1)\big) \quad \text{for } r \geq r^{**}\,. \qquad (9)$$

CB–drops on a surface with puddles are never stable because they have the advancing bounds as for W–type on a surface with puddles, i.e. $W/P = \varphi(-\cos\theta^Y + \lambda) - 1 + \varphi$. On the other hand the receding bound is as for CB–drops on a dry surface, i.e. $D/CB = \varphi(-\cos\theta^Y - \lambda) + 1 - \varphi > W/P$.

The diagrams in Figures 6–8 are plotted under the assumption $-\cos\theta^Y - \lambda < 0 < -\cos\theta^Y + \lambda$, for which $\lambda$ can be adjusted. Notice that, they show the hydrophobic case, $-\cos\theta^Y > 0$. The same diagrams hold for a hydrophilic material but with $r^* > r^{**}$. In the case $-\cos\theta^Y - \lambda > 0$, W–drops become unstable for $r > \frac{\varphi-1}{\cos\theta^Y+\lambda} + \varphi$ and puddles on the surface are never stable. For $-\cos\theta^Y + \lambda < 0$, CB–drops are never stable.

### 3.2 Quasistatic evolution

Our model describes the time evolution of a drop driven by some external force. This force is represented by moving the upper interface point in time, see Section 2.2. The system responds in two steps. First the contact angle changes, with no motion of the contact line as long as the contact angles satisfy criterion (5). Then the triple point jumps to the next cavity. Hereby it exhibits the microstructure with respect to which the contact angle became unstable. That is the microstructure which gives the relevant bound in Section 3.1.
Advancing and receding the drop more than once gives a hysteresis loop in the configurations of the drop and it finally leads to configurations that are stable with respect to further movements along the solid. The configurations shown in Figure 9 are the ones stable in this sense. To be more explicit: For fixed $r$, e.g. $r \in (r^*, r^{**})$ start with any kind of configuration, e.g. W–type on a dry surface. Then force the drop to recede. It will stay W leaving a dry surface behind. When forced to advance, however, the advancing front will turn to CB. If the whole drop starts moving, it will become a CB drop on a dry surface, and subsequent loading cycles will produce a stable (and smaller) hysteresis cycle with respect to the one exhibited during the first loading cycle.

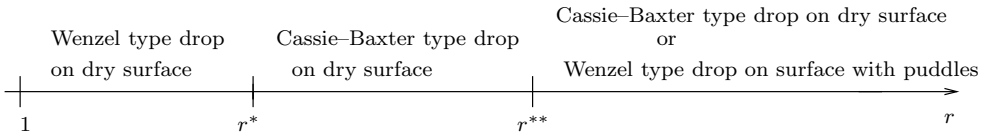


Figure 9: Stable configurations in the hydrophobic case

## 4 Connection with experiments

Figures 6 and 7 are in close qualitative agreement with the experiments in [LQ], which are done on a dry surface. The authors find a strong dependence of the stable contact angles on the type of drop: W–drops show a much stronger contact angle hysteresis than

CB–drops, which is also predicted by our model. Figure 2 shows the separation of receding contact angles depending on the pressure pushing the drop onto the surface. The authors conjecture that high pressures induce W–drops, which have low receding contact angles. Whereas low pressures lead to CB–drops with high receding contact angles. Notice that the surface material used in [LQ] satisfies the condition valid for our diagrams, namely, $-\cos\theta^Y + \lambda > 0 > -\cos\theta^Y - \lambda$, which is that the receding (resp. advancing) contact angle for the flat surface are below (resp. above) 90°.

Our model sees the metastability of CB–drops pointed out in [LQ]. Here, as well as in the more recent studies [ME] and [BM], a transition from a CB–drop to a W–drop is observed, accompanied by a decrease in the contact angle. It is by now well known that the decrease of contact angle signals a transition from a higher to a lower energy state (see [P], [AD]). Our model can reproduce this transition in so far as it allows for metastable drops. By defining $\bar{r}$ as the roughness where W and CB drops are of same energy, we get

$$\bar{r} := \frac{1-\varphi}{-\cos\theta^Y} + \varphi \; > \; r^*,$$

which leaves a range $(r^*, \bar{r})$ where CB drops are stable but do not minimize surface energy. Similarly for $r > \bar{r}$, W drops are stable in spite of their high surface energy.

The dependence of the stable contact angles on the drop type also explains the highly non–monotone behavior in Figure 1. The non–monotonicity comes from a jump in the type of drop. Figure 1 can be seen as a superposition of the diagrams in Figures 6 and 7. The choice of which diagram is valid can be done with the same arguments leading to Figure 9. For a dry surface the valid diagram changes at $r^*$, where we get a jump in the receding contact angle. This is because the hysteresis interval for a CB–drop, the stable one for $r > r^*$, is much narrower than the hysteresis interval for a W–drop, the stable type for $r < r^*$.
Note that our model predicts a roughness–induced decrease of the receding contact angle for W–drops only in the case $-\cos\theta^Y - \lambda < 0$. This is not in agreement with the experiments in [DJ], which show a reduction of the receding contact angle with roughness also for surfaces which, when flat, exhibit contact angles slightly above 90°.

Our model can also reproduce the arguments in [H], that CB–drops can even be stable on a hydrophilic surface. Figure 7 is valid independent of the sign of $\cos\theta^Y$ hence, in particular, it applies to the hydrophilic case $\cos\theta^Y > 0$. The surface then behaves as ultra–hydrophobic for CB–drops with very little microscopic contact, since $-\cos\theta^{CB} := 1-\varphi(1+\cos\theta^Y) > 0$ for small $\varphi$. Multiscale features in the surface roughness, suggested by the structure of some plants (see [BN]), are sometimes invoked to explain this phenomenon (see [H]). However, hydrophobicity may come just as well from metastable configurations with very little contact with the surface, and it is possible to induce little contact through spikes standing far apart in the surface, without multiscale asperities.

# 5 Proofs

## 5.1 Stable contact angles

We look at a fixed drop $L_0$. Without loss of generality assume $Z(L_0) = 0$. According to (4) we compare $L_0$ to all drops $\tilde{L}$ which agree with $L_0$ on the non–solid boundary of $B$. Rewrite (4) as

$$0 \leq f_{L_0}(\tilde{L}, X(\tilde{L})) := E(\tilde{L}) - E(L_0) + dist(\tilde{L}, L_0)\,. \tag{10}$$

We consider drops $\tilde{L}$ whose microstructure agrees with $L_0$ inside its contact area but $\tilde{L}$ has advanced resp. receded. The area advanced resp. receded by $\tilde{L}$ contains many cavities as we are considering macroscopic variations. Therefore

$$f_{L_0}(\tilde{L}, X(\tilde{L})) = \big(X(\tilde{L}) - X(L_0)\big)\, C(L_0, \tilde{L}) + \sqrt{1 + (X(\tilde{L}))^2} - \sqrt{1 + (X(L_0))^2}\,,$$

where $C(L_0, \tilde{L})$ is the cost (i.e., the energy difference *plus* the dissipation distance) to pay for one cavity. We estimate this cost by a suitable average, in the same spirit of the homogenized surface tensions defined in [AD], where the interfacial energy is evaluated rigorously by homogenization methods in the limit of small scale asperities.
Look at $C(L_0, \tilde{L})$ for advanced area. This does not depend on the drop type $L_0$ but on the surface (with or without puddles) and the microstructure of $\tilde{L}$ on the advanced area. There is the possibility to advance with:

1. W–type on a dry surface: $C(L_0, \tilde{L}) = r(-\cos\theta^Y + \lambda) = W/D$
2. CB–type on a dry surface: $C(L_0, \tilde{L}) = \varphi(-\cos\theta^Y + \lambda) + 1 - \varphi = CB/D$
3. W–type on a surface with puddles: $C(L_0, \tilde{L}) = -1 + \varphi + \varphi(-\cos\theta^Y + \lambda) = W/P$.

Similarly the cost for receded area does not depend on the surface type but on the microstructure of $L_0$ and the surface that is left behind:

1. W–type leave behind a dry surface: $C(L_0, \tilde{L}) = r(-\cos\theta^Y - \lambda) = D/W$
2. CB–type leave behind a dry surface: $C(L_0, \tilde{L}) = \varphi(-\cos\theta^Y - \lambda) + 1 - \varphi = D/CB$
3. W–type leave puddles behind: $C(L_0, \tilde{L}) = -1 + \varphi + \varphi(-\cos\theta^Y - \lambda) = P/W$
4. CB–type leave liquid tops behind: $C(L_0, \tilde{L}) = 1 - 2\varphi$.

These costs are the bounds for the cosines of the stable contact angles. To see this note that $f_{L_0}(L_0, X(L_0)) = 0$. We show that this is not a local minimum of $f_{L_0}$, if $-\cos\theta(L_0)$ is above resp. below $C(L_0, \tilde{L})$. This implies instability by (4) and (10).

$$\frac{d}{dX(\tilde{L})} f_{L_0}(\tilde{L}, X(\tilde{L})) = C(L_0, \tilde{L}) + \frac{X(\tilde{L})}{\sqrt{1 + (X(\tilde{L}))^2}} = C(L_0, \tilde{L}) + \cos\theta(\tilde{L}).$$

But $f_{L_0}$ has no local minimum at $L_0$ if the derivative for $X(\tilde{L}) > X(L_0)$, i.e. for advancing variations, is negative. Since we take the derivative at position $X(L_0)$ it is negative for one of the microstructures if $-\cos\theta(L_0) > \min\{C(L_0, \tilde{L})\}$. Analogously, $L_0$ is unstable with respect to receding variations if $-\cos\theta(L_0) < \max\{C(L_0, \tilde{L})\}$. This gives the bounds on the regions of stability in Section 3.1. Note that the receding bound for CB–drops which leave liquid tops behind (these configurations were suggested in [RF]) is not relevant in our model because

$$\max\{1-\varphi-\varphi(\cos\theta^Y+\lambda)\,,\,1-2\varphi\} \;=\; 1-\varphi-\varphi(\cos\theta^Y+\lambda).$$

The vertical bounds $I$ and $E$ in Section 3.1 come from interior and exterior variations. This means that we compare the drop $L_0$ with a drop $\tilde{L}$ having the same contact angle and microstructure as $L_0$ but one of the cavities interior or exterior to the contact area filled with vapor or liquid different from $L_0$. For example, for the $I$ bound, the stability criterion (4) (applied to a cavity $L_0$ filled with vapor, which is compared to a water-filled cavity $\tilde{L}$) reduces to

$$\begin{aligned} 0 \;&\leq\; E(\tilde{L}) \,-\, E(L_0) + \,dist(\tilde{L}, L_0) \\ &=\; -r\cos\theta^Y - \big(1-\varphi-\cos\theta^Y\varphi\big) + \lambda(r-\varphi)\,. \end{aligned}$$

This is satisfied if and only if

$$r \geq \frac{1-\varphi}{-\cos\theta^Y+\lambda} + \varphi = r^*\,.$$

The argument for the $E$ bound is analogous, and it leads to the inequality $r \geq r^{**}$ involving the second critical roughness coefficient $r^{**}$.

## 5.2 Quasistatic evolution

To prove that the time evolution described in 3.2 is consistent with our model we have to check (5) and (6).
Condition (5) is satisfied by construction. As long as the triple point does not move no energy is dissipated, therefore $Diss(L, [t_0, t)) = 0$. This turns (6) into:

$$E\big(t, L(t)\big) \;-\; E\big(t_0, L(t_0)\big) \;=\; \int_{t_0}^{t} \partial_t E\big(s, L(s)\big) ds,$$

which is satisfied as $E$ is $t$-differentiable. Now look at a jump, and let $t^*$ be the jump time. At $t^*$ equation (6) turns into

$$E\big(t^*, L(t^*+)\big) \;-\; E\big(t^*, L(t^*-)\big) \;+\; Diss(L, [t^*, t^*]) \;=\; 0. \tag{11}$$

By definition,

$$Diss(L, [t^*, t^*]) \;=\; dist\big(L(t^*+), L(t^*-)\big).$$

Therefore (11) is nothing but (5) written with equality, which is satisfied at the boundaries of the stability region. Here $L(t^*+)$ has the microstructure of $\tilde{L}$ with respect to which $L(t^*-)$ became unstable. Finally, notice that (6) is an additive equation.

# Acknowledgements

We thank Martin Rumpf and Julia Dohmen for valuable discussions. This work was supported by the BMBF Förderbereich Mathematik and by INdAM through the research project "Mathematical Challenges in Nanomechanics".


# References


[AD] Alberti, G., DeSimone, A., *Wetting of rough surfaces: a homogenization approach*, Proc. R. Soc. London Ser. A Math. Phys. Eng. Sci., **461**, pp. 79–97, (2005).

[BM] Bartolo, D., Bouamrirene, F., Verneuil, A., Buguin, A., Silberzan, P., Moulinet, S., *Bouncing or sricky droplets: Impalement transitions on superhydrophobic micropatterned surfaces*, Europhys. Letters **74** (2), pp. 299–305, (2006).

[BN] Barthlott, W., Neinhuis, C., *Characterization and Distribution of Water–repellent, Self–cleaning Plant Surfaces*, Annals of Botany, **79**, pp. 667–677, (1997).

[DM] Dal Maso, G., DeSimone, A., Mora, M.G., *Quasistatic evolution problems for linearly elastic–perfectly plastic materials*, Arch. Rat. Mech. Anal. **180**, pp. 237–291, (2006).

[dG] de Gennes, P.G., *Wetting: statics and dynamics*, Rev. of Mod. Physics, **57** No.3 Part I, pp.827–863, (1985).

[dBQ] de Gennes, P.G., Brochard-Wyart, F., Quéré, D., *Capillarity and Wetting Phenomena*, Springer, (2004).

[DJ] Dettre, R.H., Johnson, R.E., *Contact Angle Hysteresis II. Contact Angle Measurements on Rough Surfaces*, Contact Angle, Wettability and Adhesion, Advances in Chemistry Series, **43**, pp. 136–144, (1964).

[FM] Francfort, G., Marigo, J.J., *Revisiting brittle fracture as an energy minimization problem*, J. Mech. Phys. Solids, **50**, pp. 1319–1342, (1998).

[FG] Francfort, G., Garroni, A., *A variational view of partial brittle damage*, Arch. Rat. Mech. Anal., in press, (2006).

[H] Herminghaus, S., *Roughness–induced non–wetting*, Europhys. Letters, **52** (2), pp. 165–170, (2000).

[LQ] Lafuma, A., Quéré, D., *Superhydrophobic States*, Nature Materials, **2**, pp. 457–460, (2003).

[ME] McHale, G., Aqil, S., Shirtcliffe, N.J., Newton, M.I., Erbil, H.Y., *Analysis of evaporation on a superhydrophobic surface*, Langmuir **21**, pp. 11053–11060, (2005).

[MM] Mainik, A., Mielke, M., *Existence results for energetic models for rate–independent systems*, Calc.Var. **22**, pp. 73–99, (2005).

[M] Mielke, M., *Evolution of rate–independent systems*, Handbook of Differential Equations. Evolutionary Equations, vol. **2**, pp. 461–559, (2005).

[MT] Mielke, M., Theil, F. *On rate independent hysteresis models*, NoDEA **11**, pp. 151–189, (2004).

[P] Patankar, N., *On the Modeling of Hydrophobic Contact Angles on Rough Surfaces*, Langmuir **19**, pp. 1249–1253, (2003).

[Q] Quéré, D., *Rough ideas on wetting*, Physica A, **313**, pp. 32–46, (2002).

[RF] Roura, P., Fort, J., *Comment on " Effects of the surface roughness on Sliding Angles of Water Droplets on Superhydrophobic Surfaces"*, Langmuir **18**, pp. 566–569, (2003).

Bestellungen nimmt entgegen:

Institut für Angewandte Mathematik
der Universität Bonn
Sonderforschungsbereich 611
Wegelerstr. 6
D - 53115 Bonn

Telefon: 0228/73 3411
Telefax: 0228/73 7864
E-mail: anke@iam.uni-bonn.de Homepage: http://www.iam.uni-bonn.de/sfb611/

**Verzeichnis der erschienenen Preprints ab No. 255**

255. Albeverio, Sergio; Nizhnik, Leonid: Schrödinger Operators with Nonlocal Point Interactions

256. Albeverio, Sergio; Alimov, Shavkat: On One Time-Optimal Control Problem Associated with the Heat Exchange Process; erscheint in: Applied Mathematics and Optimization

257. Albeverio, Sergio; Pustylnikov, Lev D.: Some Properties of Dirichlet L-Functions Associated with their Nontrivial Zeros II

258. Abels, Helmut; Kassmann, Moritz: An Analytic Approach to Purely Nonlocal Bellman Equations Arising in Models of Stochastic Control

259. Gottschalk, Hanno; Smii, Boubaker; Thaler, Horst: The Feynman Graph Representation of Convolution Semigroups and its Application to Lévy Statistics

260. Philipowski, Robert: Nonlinear Stochastic Differential Equations and the Viscous Porous Medium Equation

261. Albeverio, Sergio; Kosyak, Alexandre: Quasiregular Representations of the Infinite-Dimensional Nilpotent Group

262. Albeverio, Sergio; Koshmanenko, Volodymyr; Samoilenko, Igor: The Conflict Interaction Between Two Complex Systems. Cyclic Migration.

263. Albeverio, Sergio; Bozhok, Roman; Koshmanenko, Volodymyr: The Rigged Hilbert Spaces Approach in Singular Perturbation Theory

264. Albeverio, Sergio; Daletskii, Alexei; Kalyuzhnyi, Alexander: Traces of Semigroups Associated with Interacting Particle Systems

265. Gozzi, Fausto; Marinelli, Carlo; Savin, Sergei: Optimal Advertising under Uncertainty with Carryover Effects

266. Marinelli, Carlo; D'Addona, Stefano; Rachev, Svetlozar: A Comparison of Some Univariate Models for Value-at-Risk and Expected Shortfall

267. Kassmann, Moritz: $\mathscr{S}$–Harmonische Funktionen und Sprungprozesse; erscheint in: DMV-Mitteilungen

268. Burstedde, Carsten: On the Numerical Evaluation of Fractional Sobolev Norms

269. Verleye, Bart; Klitz, Margrit; Croce, Roberto; Roose, Dirk; Lomov, Stepan; Verpoest, Ignaas: Computation of the Permeability of Textiles; erscheint in: Springer Verlag, "Computational Textile", edited by: Xianyi Zeng, Yi Li, Da Ruan, Ludovic Koehl

270. Ebmeyer, Carsten: Regularity in Sobolev Spaces of Steady Flows of Fluids with Shear-Dependent Viscosity; erscheint in: Mathematical Methods in the Applied Sciences

271. Griebel, Michael; Metsch, Bram; Schweitzer, Marc Alexander: Coarse Grid Classification – Part II: Automatic Coarse Grid Agglomeration for parallel AMG

272. Chen, Kai; Albeverio, Sergio; Fei, Shao-Ming: Tight Bell Inequalities for many Qubits

273. Husseini, Ryad; Kassmann, Moritz: Jump Processes, $\mathscr{S}$-Harmonic Functions, Continuity Estimates and the Feller Property

274. Otto, Felix; Reznikoff, Maria G.: A New Criterion for the Logarithmic Sobolev Inequality

275. Otto, Felix; Reznikoff, Maria G.: Slow Motion of Gradient Flows

276. Albeverio, Sergio; Baranovskyi, Oleksandr; Pratsiovytyi, Mykola; Torbin, Grygoriy: The Ostrogradsky Series and Related Probability Measures

277. Albeverio, Sergio; Koroliuk, Volodymyr; Samoilenko, Igor: Asymptotic Expansion of Semi-Markov Random Evolutions

278. Frehse, Jens; Kassmann, Moritz: Nonlinear Partial Differential Equations of Fourth Order under Mixed Boundary Conditions

279. Juillet, Nicolas: Geometric Inequalities and Generalized Ricci Bounds in the Heisenberg Group

280. DeSimone, Antonio; Grunewald, Natalie; Otto, Felix: A New Model for Contact Angle Hysteresis